Mutational and Structural Studies of the Diisopropylfluorophosphatase from *Loligo vulgaris* Shed New Light on the Catalytic Mechanism of the Enzyme†

Vicky Katsemi,‡,§ Christian Lücke,‡,|| Juergen Koepke,⊥ Frank Löhr,‡ Steffen Maurer,‡ Günter Fritzsch,⊥ and Heinz Rüterjans*,‡

Institute of Biophysical Chemistry, Center for Biomolecular Magnetic Resonance, J. W. Goethe University of Frankfurt, Marie-Curie-Strasse 9, and Department of Molecular Membrane Biology, Max Planck Institute of Biophysics, Marie-Curie-Strasse 15, 60439 Frankfurt am Main, Germany

Received January 12, 2005; Revised Manuscript Received April 5, 2005

ABSTRACT: The active site, the substrate binding site, and the metal binding sites of the diisopropylfluorophosphatase (DFPase) from *Loligo vulgaris* have been modified by means of site-directed mutagenesis to improve our understanding of the reaction mechanism. Enzymatic characterization of mutants located in the major groove of the substrate binding pocket indicates that large hydrophobic side chains at these positions are favorable for substrate turnover. Moreover, the active site residue His287 proved to be beneficial, but not essential, for DFP hydrolysis. In most cases, hydrophobic side chains at position 287 led to significant catalytic activities although reduced relative to the wild-type enzyme. With respect to the Ca-1 binding site, where catalysis occurs, various mutants indicated that the net charge at this calcium-binding site as well as the relative positions of the charged calcium ligands is crucial for catalytic activity. The importance of the electrostatic potential at the active site was furthermore revealed by various mutations of residues lining the interior of the central water-filled tunnel, which traverses the entire protein structure. In this respect, the structural features of residue His181, which is located at the opposite end of the DFPase tunnel relative to the active site, were characterized extensively. It was concluded that a tunnel-spanning hydrogen bond network, which includes a large number of apparently slow exchanging water molecules, relays any modifications in the electrostatics of the system to the active site, thus affecting the catalytic reactivity of the enzyme.

The calcium metalloenzyme diisopropylfluorophosphatase (DFPase)[1] from *Loligo vulgaris* catalyzes the hydrolysis of diisopropyl fluorophosphate (DFP) and related acetylcholinesterase inhibitors (*1*−*4*), as schematically presented in Figure 1. Consequently, DFPase has generated considerable interest for bioremediation applications due to its proven potential for the rapid and complete detoxification of organophosphate nerve agents such as DFP, sarin, cyclohexylsarin, soman, and tabun. There are several known enzymes that hydrolyze such chemical warfare agents, but only DFPase and a phosphotriesterase from *Pseudomonas diminuta* can be expressed in sufficiently high yields and are capable of decontamination with high turnover numbers (*5*, *6*). The natural biological functions of these enzymes still remain unknown in most cases, except for human paraoxonase 1 (PON1), which is thought to be a component of the high-density lipoprotein particles and to be associated with the inactivation of toxic products that are generated during oxidation of lipidic components by the low-density lipoprotein complex (*7*, *8*). Moreover, an organophosphate-hydrolyzing enzyme isolated from two different *Alteromona*s species is considered to be a member of the prolidase family (*9*, *10*).

The squid-type DFPase from *L. vulgaris* (EC 3.1.8.2; 35 kDa molecular mass) consists of 314 amino acids and two calcium-binding sites (*3*). Scharff and co-workers have succeeded in crystallizing recombinant DFPase (*11*) and determining its structure to a final resolution of 0.85 Å (*12*). The DFPase has a β-propeller structure that comprises six propeller blades. They are arranged in a 6-fold pseudosymmetry around a central water-filled tunnel that contains both calcium ions. One metal ion has been identified as the "low-affinity" calcium (Ca-1), which plays a crucial role in enzymatic catalysis (*1*, *3*), whereas the "high-affinity" calcium (Ca-2) is responsible for the structural stability of the enzyme, as incubation with chelating agents results in an irreversible inactivation of DFPase. Biophysical and site-directed mutagenesis studies have indicated that one particular histidine residue, His287, may be essential for the hydrolytic reaction (*4*). According to the X-ray structure

† This work has been supported by the Fraunhofer Gesellschaft (Grant E/E590/3X023/M5137).

* To whom correspondence should be addressed. Phone: +49-69-79829622. Fax: +49-69-79829632. E-mail: hruet@bpc.uni-frankfurt.de.

‡ J. W. Goethe University of Frankfurt.

§ Present address: Hellenic Pasteur Institute, Department of Biochemistry, Vas. Sofias 127, 11521 Athens, Greece.

|| Present address: Max Planck Research Unit for Enzymology of Protein Folding, Weinbergweg 22, D-06120 Halle, Germany.

⊥ Max Planck Institute of Biophysics.

[1] Abbreviations: COSY, correlated spectroscopy; DFP, diisopropyl fluorophosphate; DFPase, diisopropylfluorophosphatase; E.COSY; exclusive correlation spectroscopy; HMBC, heteronuclear multiple bond correlation; NOESY, nuclear Overhauser and exchange spectroscopy; PON, human paraoxonase; TROSY, transverse relaxation optimized spectroscopy; WT, wild type.

10.1021/bi0500675 CCC: $30.25
Published on Web 06/02/2005

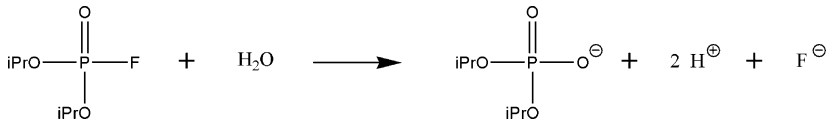

FIGURE 1: Schematic representation of the DFP hydrolysis reaction. The resulting hydrogen and fluoride ions can be detected with selective electrodes for quantitative analysis of the enzymatic activity.

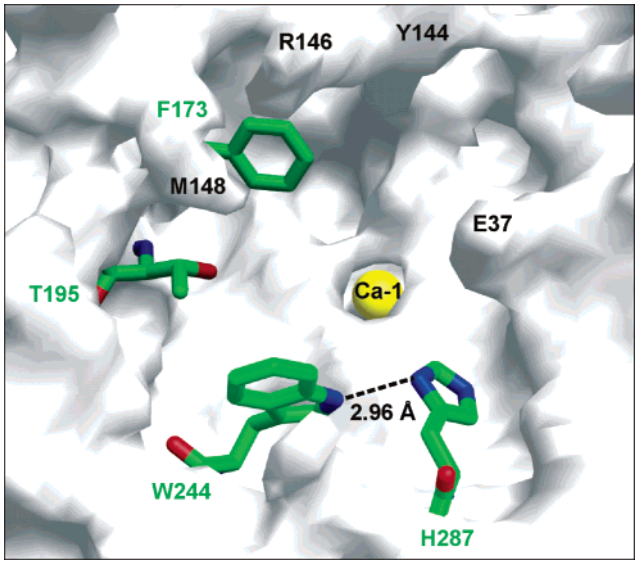

FIGURE 2: Surface representation of the DFP binding pocket in the active site of WT DFPase, with Phe173, Thr195, Trp244, and His287 shown as rods. The major binding groove is bounded by Phe173 and Trp244. The hydrogen bridge between Trp244 and His287 is indicated by the dashed line. Several other residues surrounding the active site are labeled in black. [This picture was created with the program GRASP (*16*).]

(*1*, *12*), both His287 and Ca-1 are located in a solvent-accessible surface pocket of DFPase (Figure 2). His287 $N^{\delta 1}$ is hydrogen bonded to Trp244 $N^{\epsilon 1}H$, whereas His287 $N^{\epsilon 2}H$ forms a hydrogen bond with the backbone carbonyl oxygen of Ala20. In such an arrangement, however, His287 is unable to activate the hydrolytic water molecule. Therefore, structural rearrangements in the active site appear to be necessary for the enzymatic cleavage reaction to proceed. According to the proposed catalytic mechanism of DFPase (*1*), the catalytic reaction begins with the entry of the DFP substrate into the narrow and elongated surface pocket at the active site, where the phosphoryl oxygen displaces the surface-bound water molecule WAT524 (formerly WAT45; from here on the solvent molecule numbering in this paper refers only to PDB ID code 1PJX) as a ligand to Ca-1. At the same time, the partial positive charge of the phosphorus atom is increased, thus facilitating the nucleophilic attack by the hydrolytic water molecule. This water molecule may be activated via proton abstraction by His287 when the imidazole ring is disengaged from the hydrogen bond interactions with Trp244 and Ala20, leading to a nucleophilic attack of the subsequently released hydroxyl ion on the phosphorus atom of the bound substrate. At this point, the double-protonated His287 side chain interacts with the negatively charged Glu37, while the transition state of the cleavage reaction is represented by a trigonal bipyramid configuration of the substrate. Finally, the cleaved fluoride ion is released in the opposite direction of the attacking water, possibly stabilized by the formation of a hydrogen bond with the NH_2 group of Asn120, and the hydrolyzed substrate detaches from Ca-1. After deprotonation of the charged His287, the hydrogen bond interaction with Trp244 may be restored to initiate a new reaction cycle.

The function of the central tunnel (*1*, *12*) has not been investigated to date. Ca-2, which has been characterized as the high-affinity calcium ion because of its solvent-inaccessible location and its low dissociation constant (*1*, *2*), is buried near the midpoint of this tunnel. In addition, crystal waters form an intricate hydrogen bond network throughout the tunnel, which apparently plays a role both in the structural stability and in the catalytic activity of the enzyme, as we will show in this study.

To further elucidate the above-described catalytic mechanism of the DFPase (*1*) and to identify any additional residues that may be involved in substrate binding and/or hydrolysis, a series of single and double mutants of DFPase have been generated. All mutation sites are located either around the active site or inside the central tunnel, with the aim (i) to reevaluate the role of His287 on enzymatic catalysis, (ii) to reveal the significance of several other residues localized in the substrate binding site, and (iii) to emphasize the role of the water-filled tunnel on enzymatic catalysis. To this end, the mutants were designed either to enlarge the substrate binding pocket, to alter the hydrophobic character of the active site, to interrupt the network of water molecules inside the tunnel, or to change the electrostatic potential at one of the metal binding sites.

MATERIALS AND METHODS

Expression, Purification, and Crystallization of Recombinant DFPase. The recombinant squid-type DFPase has been expressed, purified, and characterized as described elsewhere (*2*−*4*). Briefly, the enzyme was expressed in *Escherichia coli* cells carrying the pKKHisND plasmid that encoded for DFPase from *L. vulgaris* (*2*). The purification occurred via metal-affinity chromatography on Ni^{2+}-NTA (Qiagen, Hilden, Germany), rechromatography on Ni^{2+}-NTA after thrombin cleavage of the His tag, and final anion-exchange chromatography on Q-Sepharose HP (Pharmacia, Uppsala, Sweden). Crystals were grown using the hanging drop vapor diffusion technique, as described previously (*11*).

Site-Directed Mutagenesis. Site-directed mutants were produced by using the QuickChange site-directed mutagenesis kit (Stratagene, Heidelberg, Germany). The mutagenic primers were obtained from MWG Biotech (Ebersberg, Germany). The sequences of the oligonucleotides are described in the Supporting Information (Table S1). The DNA sequences of all mutants were checked using the Taq DyeDesoxy terminator cycle sequencing kit (Applied Biosystems, Weiterstadt, Germany).

Expression, purification, and crystallization of the mutants were carried out as for the wild-type (WT) enzyme, except that the precipitant size varied from PEG 4000 to PEG 10000, the precipitant content varied between 12% and 13% PEG, and the pH varied between 6.0 and 6.5.

Enzymatic Activity Assays. The enzymatic activities of the WT and mutant enzymes were determined at room temperature by two independent procedures that have been described previously (*3*), i.e., either by fluoride ion detection or by pH titration. In short, the fluoride assays were performed in a total volume of 5 mL, with the assay solution consisting of 0.5 M NH_4HCO_3 (pH 7.5) and 5 mM DFP. The release of fluoride ions was monitored with a fluoride ion-selective electrode coupled to a pHM 240 pH-ion meter (Radiometer, Kopenhagen, Denmark). After addition of enzyme, the reaction was monitored for 15 min. Alternatively, the pH assays were performed in a total volume of 3 mL under nitrogen atmosphere, with the assay solution consisting of 10 mM NaCl and 5 mM DFP set to pH 7.5. The protons released by the DFP cleavage reaction were titrated with a 10 mM NaOH solution using a "pH-stat" equipment (Radiometer, Kopenhagen, Denmark). After addition of enzyme, the reaction was monitored for 10 min.

The spontaneous hydrolysis rate of DFP in the absence of enzyme (below 0.2 μmol of DFP/min) was determined under identical conditions for each series of measurements and subsequently subtracted from the enzymatic hydrolysis rates in the presence of enzyme. The resulting enzymatic activities were obtained as units per milliliter, where 1 unit is defined as the hydrolysis of 1 μmol of DFP/min; specific activities are expressed as units per milligram of protein.

TXRF Measurements. The calcium ion stoichiometry of each DFPase mutant was determined with total-reflection X-ray fluorescence analysis (TXRF) using standard procedures.

X-ray Data Collection. X-ray data were collected at the synchrotron beamlines BW7A and BW7B of the EMBL, Hamburg Outstation, and at the synchrotron beamline DW32 of Lure, Paris. The data sets were processed with DENZO of the HKL program suite (*13*, *14*). Data were merged using SCALEPACK. Structure factors were calculated from the measured intensities by employing TRUNCATE of the CCP4 package (*15*). The structural refinement was carried out as described elsewhere (*1*). Structures were graphically analyzed by using the program INSIGHT (Accelrys, San Diego, CA). Atom potentials were calculated with GRASP version 1.2.5 (*16*).

NMR Experiments. The NMR experiments of WT DFPase were performed in 10 mM 1,3-bis[tris(hydroxymethyl)-methylamino]propane buffer (pH 6.5), supplemented with 5 mM $CaCl_2$, 0.02% sodium azide, 50 μg/mL Pefabloc protease inhibitor, 0.15 mM 4,4-dimethyl-4-silapentane-1-sulfonate (DSS), which was used as internal chemical shift standard, and 5−10% D_2O. Data were collected at a sample temperature of 28 °C on Bruker DMX 600 or AVANCE 900 spectrometers, equipped with three-axis gradient $^1H\{^{13}C,^{15}N\}$ triple resonance probes.

For qualitative structure analysis, standard 1D ^1H NMR spectra or 2D [^{15}N,^1H]-TROSY spectra were acquired, employing nonlabeled or uniformly ^{15}N-labeled DFPase samples, respectively, as previously described (*17*).

For pH-titration analysis of WT DFPase, [^{15}N,^1H]-HMBC and [^{15}N,^1H]-TROSY spectra were recorded with U-^{15}N-labeled DFPase samples (1.35 mM) at 11 different pH values ranging from pH 5.76 to pH 9.45. The quoted pH values represent mean values of pH measurements performed before and after NMR data collection at each titration point. The pH titration was started with two identical protein samples, one at pH 5.76 and the other at pH 9.45. The subsequent titration steps were achieved by the addition of small volumes (20−100 μL) from one sample to the other.

For the detection of trans-hydrogen-bond scalar couplings, a 1 mM sample (300 μL) of U-^2H,^{15}N-labeled DFPase was placed in a Shigemi microcell. The applied 2D pulse sequences were of the TROSY (*18*) type and employed a gradient echo/antiecho coherence-selected, sensitivity-enhanced detection scheme (*19*−*22*). In both [^{15}N,^1H]-TROSY-H(N)N-COSY quantitative *J*-correlation (*23*) and $^1H-S^3$ [^{15}N,^1H]-TROSY-H(N)N-COSY (*24*−*26*) experiments the Δ periods for evolution of $^{15}N-^{15}N$ scalar couplings were adjusted to 40 ms. To account for the large chemical shift difference of backbone amide and nonprotonated histidine ring nitrogens, the rectangular ^{15}N refocusing pulses in the center of Δ were replaced by pairs of 1.5 ms WURST-20 (*27*) adiabatic pulses (40 kHz sweep), applied at $\Delta/4$ and $3\Delta/4$, and the ^{15}N carrier frequency was positioned at 152 ppm. In the E.COSY [^{15}N,^1H]-TROSY experiment (*28*), the ^{15}N carrier was centered in the backbone amide region and the widths of rectangular 90° and 180° ^{15}N pulses were adjusted to provide a null in their excitation profile at the His181 $^{15}N^{\epsilon 2}$ resonance (249 ppm). Spectral widths in the [^{15}N,^1H]-TROSY-H(N)N-COSY experiment (recorded at 900 MHz) were 10.0 ppm in the ^1H dimension (carrier frequency placed at 9.2 ppm) and 219.2 ppm in the ^{15}N dimension. Time domain data sizes were 256 (t_1) × 768 (t_2) complex points, corresponding to acquisition times of 12.8 and 85.4 ms, respectively. The experiment was recorded within 2 h using four scans for each FID. In the $^1H-S^3$ [^{15}N,^1H]-TROSY-H(N)N-COSY experiment (600 MHz ^1H frequency) for the determination of $^{h1}J_{HN}$, two data sets, where either TROSY or anti-TROSY components were selected during t_1, were recorded in an interleaved manner using spectral widths of 17.1 (carrier frequency at the H_2O resonance) and 228.4 ppm in the ^1H and ^{15}N dimensions, respectively. Acquisition times were 73.7 (t_1, 1024 complex points) and 75.0 ms (t_2, 768 complex points). Sixteen transients were accumulated for each FID, giving rise to a total measurement time of 40 h. The E.COSY [^{15}N,^1H]-TROSY experiment was recorded at 900 MHz ^1H frequency with spectral widths of 18.0 ppm (^1H dimension, carrier frequency at the H_2O resonance) and 27.0 ppm (^{15}N dimension). Acquisition times were 284.2 ms (t_1, 700 complex points) and 126.4 ms (t_2, 2048 complex points). Using four scans per FID, the recording time was 8.5 h. Processing of the spectra was performed with Bruker XWIN-NMR (version 2.6) software. Prior to zero-filling and Fourier transformation, the time domain data of the [^{15}N,^1H]-TROSY-H(N)N-COSY experiments were apodized with squared cosine functions in both dimensions. For the E.COSY [^{15}N,^1H]-TROSY data set, squared sine functions, shifted by $\pi/3$ and $\pi/16$, were employed in the ^1H and ^{15}N dimensions, respectively.

RESULTS AND DISCUSSION

Active Site. As stable complexes of DFPase with either substrate or inhibitor are not known to date, the structural and functional role of residues in the active site had to be investigated by site-directed mutagenesis. To this end, point mutations have been introduced to the active site that were aimed on one hand at enlarging the substrate binding pocket and on the other hand at increasing its hydrophobic character.

Table 1: Specific Activities and Calcium Content of Newly Generated DFPase Mutants

	specific activity				
			mean value		
DFPase mutant	pH[a] (units/mg)	fluoride[a] (units/mg)	abs (units/mg)	rel to WT (%)	Ca^{2+} content per protein[b]
WT	208 ± 13 (220)	180 ± 14 (268)	194	100	2.1 ± 0.2
Q77F	0 (5)	0 (5)	0	0	4.3 ± 0.4
Q77W	205 ± 18 (6)	180 ± 17 (6)	193	106	2.3 ± 0.3
Q77Y	182 ± 14 (6)	165 ± 17 (6)	174	94	2.1 ± 0.3
N120D	9 ± 2 (6)	5 ± 1 (14)	7	4	2.8 ± 0.2
D121F	0 (5)	0 (5)	0	0	0.9 ± 0.3
Y144S	224 ± 17 (6)	193 ± 18 (6)	209	108	2.2 ± 0.3
R146S	100 ± 9 (6)	112 ± 9 (7)	106	55	2.1 ± 0.3
M148A	148 ± 10 (6)	137 ± 12 (18)	143	74	1.9 ± 0.2
F173A	34 ± 5 (6)	28 ± 6 (10)	31	16	2.2 ± 0.2
F173L	160 ± 12 (6)	126 ± 13 (18)	143	72	1.9 ± 0.3
F173S	83 ± 7 (8)	43 ± 6 (15)	63	32	1.9 ± 0.3
F173V	119 ± 10 (6)	92 ± 10 (9)	105	54	2.0 ± 0.1
F173W	164 ± 11 (10)	151 ± 14 (6)	158	81	2.3 ± 0.3
F173Y	125 ± 8 (9)	58 ± 8 (5)	92	47	2.1 ± 0.2
N175D	4 ± 1 (6)	3 ± 2 (12)	4	2	2.3 ± 0.2
H181N[c]				81	2.1 ± 0.4
T195A	82 ± 7 (6)	65 ± 6 (7)	78	40	1.6 ± 0.3
T195L	186 ± 13 (7)	160 ± 12 (7)	173	89	1.9 ± 0.2
T195V	209 ± 16 (6)	166 ± 14 (9)	188	97	2.2 ± 0.3
D229N/N120D	0 (5)	0 (5)	0	0	1.8 ± 0.1
D232S	213 ± 13 (7)	185 ± 11 (13)	200	103	2.0 ± 0.3
S271A/D232S	183 ± 15 (6)	134 ± 12 (5)	158	81	1.9 ± 0.2
N237S	187 ± 17 (6)	162 ± 15 (5)	187	96	1.8 ± 0.3
S271A[d]				134	1.8 ± 0.1
N272F	0 (5)	0 (5)	0	0	0.7 ± 0.3
H274N[c]				93	2.0 ± 0.2
H287A	17 ± 3 (7)	21 ± 4 (5)	19	10	2.0 ± 0.1
H287D[e]				1	1.8 ± 0.3
H287F	131 ± 10 (11)	117 ± 9 (10)	124	64	1.8 ± 0.2
H287L	149 ± 10 (6)	159 ± 12 (5)	154	79	2.2 ± 0.3
H287N[c]				4	2.0 ± 0.3
H287Q	141 ± 11 (6)	39 ± 6 (5)	90	46	2.0 ± 0.3
H287W	150 ± 12 (7)	107 ± 11 (6)	129	66	2.4 ± 0.4
H287Y	91 ± 8 (6)	77 ± 9 (5)	84	43	1.9 ± 0.2
Q304F	108 ± 9 (6)	86 ± 7 (5)	97	50	2.0 ± 0.1
Q304W	205 ± 18 (6)	170 ± 13 (5)	188	97	1.8 ± 0.3
F314A	203 ± 14 (5)	195 ± 16 (9)	199	103	2.2 ± 0.3

[a] The number of independent pH and fluoride measurements is indicated in parentheses. [b] The TXRF values were based on five different preparations of every mutant, with up to four measurements for each sample. [c] Taken from ref *3*. [d] Taken from ref *1*. [e] E. I. Scharff, personal communication.

As deduced from computer-aided modeling of DFP into the active site, the two hydrophobic isopropyl side chains of DFP are oriented in opposite directions inside the DFPase surface pocket, with one isopropyl group positioned in the major groove between the aromatic rings of Phe173 and Trp244 (Figure 2), while the other isopropyl group is placed in the vicinity of Pro36, Ile62, and Ala74 (*1*). The introduction of less hydrophobic residues in the binding pocket commonly reduces the substrate affinity, as in the case of phosphotriesterase from *P. diminuta*, where the substitution of a tryptophan residue with an alanine led to a decrease of the substrate affinity by a factor of 6 (*29*, *30*). In the case of squid-type DFPase, a similar finding has been obtained; on the basis of a series of Trp244 mutants, we had concluded previously (*1*) that residue 244 (i) needs to be highly hydrophobic in order to support the substrate binding via hydrophobic interactions and (ii) favors the formation of a hydrogen bond with the imidazole ring of His287.

The phenyl ring of Phe173 is positioned opposite to the Trp244 indole ring in the larger isopropyl binding groove (Figure 2). In the X-ray structure of WT DFPase, it was observed that the hydrophobic Phe314 side chain of one DFPase molecule projects into the active site of the adjacent DFPase molecule, with the Phe314 ring inserted into the major groove between Trp244 and Phe173, as would be expected for one isopropyl group of the DFP substrate (*1*). Attempts to free the occupied binding pocket to allow substrate binding by replacing Phe314 with an alanine residue have failed thus far; the mutant F314A exhibits the same specific activity as the WT enzyme (Table 1) and did not provide any complex structures upon crystal soaking or cocrystallization with potential inhibitor molecules.

To analyze the significance of hydrophobicity and side chain size at position 173, the mutants F173A, F173L, F173S, F173V, F173W, and F173Y have been generated (Table 1). Analysis of the specific activities of these mutants indicates that the catalytic activity generally becomes smaller with decreasing hydrophobicity of the amino acid side chains (Phe/Trp > Leu > Val/Tyr > Ala). Only the higher specific activity of the mutant F173S (32%), compared to the mutant F173A (16%), does not completely match this trend. Nevertheless, the analysis of all six Phe173 mutants indicates that larger hydrophobic residues at position 173 yield a higher enzymatic activity.

Another residue located in the major groove is Thr195 (Figure 2). Substitution of this residue with a more hydrophobic valine or leucine side chain did not significantly affect the specific activity of DFPase (Table 1). The introduction of the considerably smaller and less hydrophobic alanine side chain at the position 195, on the other hand, resulted in a 60% decrease of the catalytic activity compared to the WT protein.

In addition, we also reduced the side chain sizes of several residues located at the entrance to the active site (Figure 2). In one case (Y144S) this modification resulted in a slight increase in activity, whereas the other two mutants (R146S and M148A) exhibited activities reduced by 45% and 26%, respectively, compared to the WT enzyme. The decreased activity of the mutant R146S might be explained by the loss of a positive charge at the entrance to the active site, which may guide the substrate to the Ca-1 binding site. Certainly, the relatively small effects in activity observed for the mutants Y144S and M148A demonstrate that shorter side chains at the entrance to the active site do not provide the intended increase in the DFP turnover.

Role of His287 in the Catalytic Mechanism. Enzymatic, TXRF, and CD measurements of the mutant H287N had demonstrated earlier that His287 has a functional role in the DFPase-catalyzed hydrolysis of DFP (*3*). To better analyze the catalytic mechanism and in particular the role of His287 on the substrate turnover, a number of new mutants have now been generated and analyzed. Thereby, the following criteria, which were pointed out previously as relevant to His287 (*1*), have been focused on: (i) the ability of residue 287 to form a hydrogen bond with Trp244; (ii) the hydrophobic character of residue 287.

The exchange of His287 against phenylalanine, tryptophan, and leucine led to a reduction of the specific activity by 36%, 34%, and 21%, respectively, compared to WT DFPase (Table 1). The exchange of His287 against tyrosine, on the other hand, resulted in a more pronounced reduction of the specific activity by 57%. Since tyrosine is less hydrophobic than phenylalanine, tryptophan, or leucine, the analysis of the specific activities of the mutants H287F, H287L, H287W, and H287Y indicates that again the hydrophobicity, but not the aromaticity, at position 287 is important for the enzymatic activity of DFPase. The fact that all of these mutants exhibit a significant enzymatic activity, although less active than the WT protein, furthermore shows that residue 287 does influence the substrate binding and/or catalysis.[2] However, since all four of these mutants are highly unlikely to activate the hydrolytic water molecule by proton abstraction, we conclude that His287 may be beneficial to the activation of the hydrolytic reaction, but it is not crucial for DFP catalysis to occur. Second, the hydrogen bond between $N^{\delta 1}$ of His287 and $N^{\epsilon 1}H$ of Trp244 (Figure 2) is apparently not essential for DFP hydrolysis, contrary to our previous hypothesis (*1*), but it may reduce the polarity of the His287−Trp244 system to make this part of the active site yet more hydrophobic. In fact, NMR-based pH-titration experiments revealed that the His287 imidazole ring does not titrate within the scanned pH range 5.76−9.45 (Table 2). Moreover, slowed proton exchange was observed for $N^{\epsilon 2}H$ of His287 between pH 8.63 and pH 9.45, indicating that this residue is well shielded, at least under basic conditions.

Table 2: NMR-Derived Properties of the DFPase Histidine Residues within the pH Range 5.76−9.45

residue	protonation state	pH titration effects	slowed proton exchange
H181	$N^{\delta 1}H$	none	pH 6.45−9.04
H219	$N^{\epsilon 2}H$	below pH 7	none
H224	$N^{\epsilon 2}H$	below pH 7	none
H248	$N^{\delta 1}H$	below pH 7	pH 7.89−9.45
H274	$N^{\epsilon 2}H$	none	pH 5.76−9.04
H287	$N^{\epsilon 2}H$	none	pH 8.63−9.45

The importance of the relative size of an aliphatic hydrophobic residue at position 287 has been further tested by the preparation of the mutant H287A. This substitution resulted in a massive reduction of the enzymatic activity by 90% (Table 1), again indicating that a larger hydrophobic side chain is beneficial for substrate binding and/or turnover.

The introduction of an aspartate or asparagine at position 287 also resulted in almost complete enzyme inactivation (Table 1). In principle, the $O^{\delta 1}$ atom of asparatate or asparagine could be located at the position where the $N^{\delta 1}$ atom of the imidazole ring of His287 is positioned in the WT structure, thus maintaining the hydrogen bond to Trp244. The loss of catalytic activity of the mutants H287N and H287D should therefore be mainly due to the hydrophilic character of their side chains; they might even interact with the hydrolytic water molecule through hydrogen bonds and thereby negatively affect its activation. Hence, the nucleophilic attack of the hydrolytic water on the phosphorus atom of the substrate may in fact be favored by a hydrophobic milieu, where the solvent molecule is not bound via polar interactions.

Finally, the mutant H287Q shows a similar enzymatic activity as H287Y. Both mutants are less hydrophobic than phenylalanine, tryptophan, or leucine but more hydrophobic than aspartate or asparagine. Moreover, just like His287, the mutant H287Q could in principle form both hydrogen bonds, to Trp244 $N^{\epsilon 1}H$ and to the backbone oxygen atom of Ala20, thus rendering the entire Trp244−Gln287−Ala20 system less polar.

To exclude conformational changes as a source of the significant loss in catalytic activity observed for H287A, H287D, H287N, and H287Q, we checked the calcium content of all mutants by TXRF measurements. Unfolded DFPase mutants usually showed a Ca^{2+} content different from the WT protein; this was not the case here. Moreover, the mutant H287N had previously also been characterized by CD spectroscopy (*3*). Efforts have been made to crystallize the available His287 mutants, but only the mutant H287A could be successfully crystallized and its structure solved to a resolution of 1.07 Å.

The structure of the mutant H287A showed little conformational differences compared to WT DFPase (Figure 3). In addition to the removal of the His287 imidazole ring, the position of the Ala287 Cβ atom is shifted by 0.44 Å relative to His287 C$^{\beta}$. Second, the side chain carboxyl group of Glu37 is rotated by about 50° and shifted by 1.50 Å. Third, the

[2] As the interpretation of the kinetic parameters that have been determined for a number of DFPase mutants (see Table S2 in the Supporting Information) was rather inconclusive, we proceeded to evaluate the specific activities only.

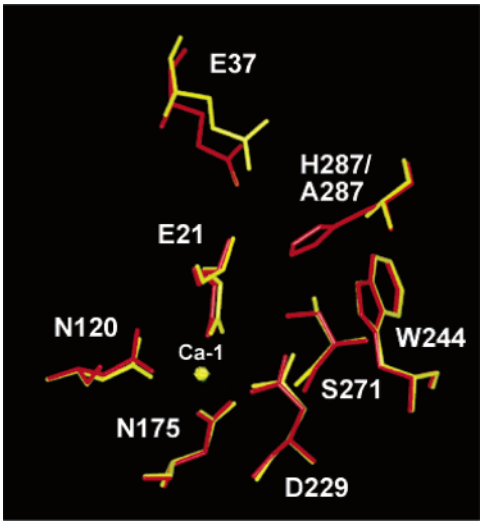

FIGURE 3: Superposition of the WT DFPase (red) and the H287A (yellow) X-ray structures. Several residues located near the point mutation in the active site are displayed as rods. [This picture was created with the program GRASP (*16*).]

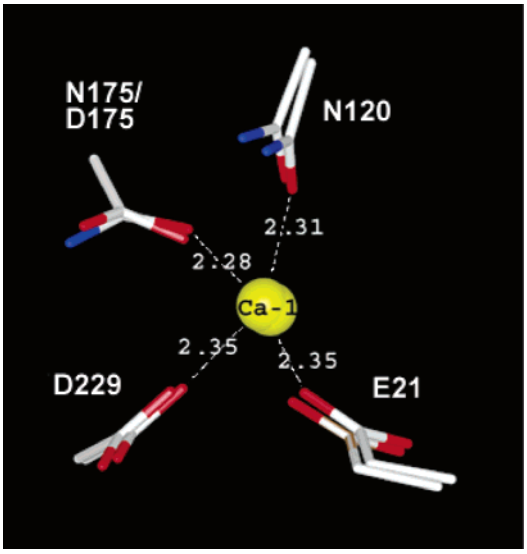

FIGURE 4: Superposition of the WT DFPase and the N175D X-ray structures. The protein ligands of Ca-1 are displayed as rods. Numbers represent distances (in Å) in the WT structure. [This picture was created with the program GRASP (*16*).]

Ca-1 is shifted by 0.35 Å. It is furthermore interesting to note that Ser271 exists in two distinct conformational states: one conformation is identical to the WT structure, whereas in the second conformation the Ser 271 O^{γ} is rotated by 90°. The larger conformational space thus occupied by the Ser271 side chain can be explained by the absence of the bulky His287 imidazole ring. Also remarkable is the rearrangement of the Glu37 side chain, since this residue is supposed to stabilize the positively charged His287 residue during catalysis via electrostatic interactions; of course, such an interaction cannot occur in the mutant H287A.

Ca-1 Binding Site. The low-affinity calcium-binding site of the DFPase (Ca-1) is essential for the catalytic activity of the enzyme (*2*). It appears to be responsible for the binding and orientation of the substrate in the active site of DFPase via electrostatic interactions. The Ca-1 atom is located at the upper entrance of the central DFPase tunnel, where it is coordinated to the side chain oxygens of Glu21, Asn120, Asn175, and Asp229 as well as three water molecules, WAT502, WAT524, and WAT604 (*1*).

To investigate the role of Ca-1 in the catalysis reaction more closely, we produced mutations of the directly liganded residues. Previously, the mutants E21Q and D229N showed a complete lack of enzymatic activity, containing only one calcium atom per protein molecule (*1*). The X-ray structure of mutant E21Q and the CD spectrum of mutant D229N, however, indicated no structural changes due to these mutations. It was therefore concluded that a reduction of the negatively charged ligands from 2 to 1 causes a complete loss of Ca-1 and subsequently all enzymatic activity.

To test the effects of an increased number of negatively charged ligands, we now prepared the mutants N120D and N175D. The specific activities of these mutants amounted to only 4% and 2%, respectively (Table 1). Moreover, the mutant N120D contained 2.8 calcium ions per protein molecule, suggesting that in this particular case the introduction of a third carboxylate group in the Ca-1 binding site resulted in the binding of an additional Ca^{2+} ion, whereas the mutant N175D contained only two calcium ions per protein molecule like WT DFPase.

The mutant N175D has been successfully crystallized and its structure solved to a resolution of 1.7 Å. The overall structural fold showed no significant differences compared to WT DFPase, with the geometry of the Ca-1 binding site basically unaltered (Figure 4). Hence, the analysis of the N175D structure revealed that not conformational but again electrostatic changes are responsible for the activity loss of this mutant.

Next, a double mutant (D229N/N120D) has been generated, exchanging the charges of two Ca-1 ligands but leaving the net charge unaltered. According to the TXRF measurements, this double mutant contains two Ca^{2+} ions per protein molecule like the WT DFPase, but the activity measurements showed that it is completely inactive. The one-dimensional ^{1}H NMR spectrum (see Figure S1 in the Supporting Information) of this double mutant was similar to that of the WT protein, indicating that the tertiary structure of the mutant has been maintained. Hence, not only the net charge at the Ca-1 binding site is important for the catalytic activity, but also the relative position of each charge plays a crucial role for the functionality of the enzyme. Apparently, the DFP catalysis is dependent on the electrostatic potential at the Ca-1 binding site, which is defined by the charges of the individual Ca-1 ligands as well as by effects relayed through the hydrogen bond network in the central tunnel of the DFPase, as will be discussed below.

Tunnel Segment between Ca-1 and Ca-2. The two calcium-binding sites, which are 9.43 Å apart, are connected by a hydrogen bond network that extends throughout the central water-filled tunnel of squid-type DFPase (Figure 5a). From Ca-1 to Ca-2 this hydrogen bond network passes between the functional groups of residues Asp121 and Asn272 (Figure 5b).

Asp121 forms a hydrogen bridge with the Ca-1 ligand WAT604, whereas Asn272 coordinates both the Ca-1 ligand Glu21 and the Ca-2 ligand WAT623. The phenylalanine mutants D121F and N272F were both completely inactive, containing only one calcium atom per protein molecule. Still, one-dimensional ^{1}H NMR spectra (see Figure S1 in the

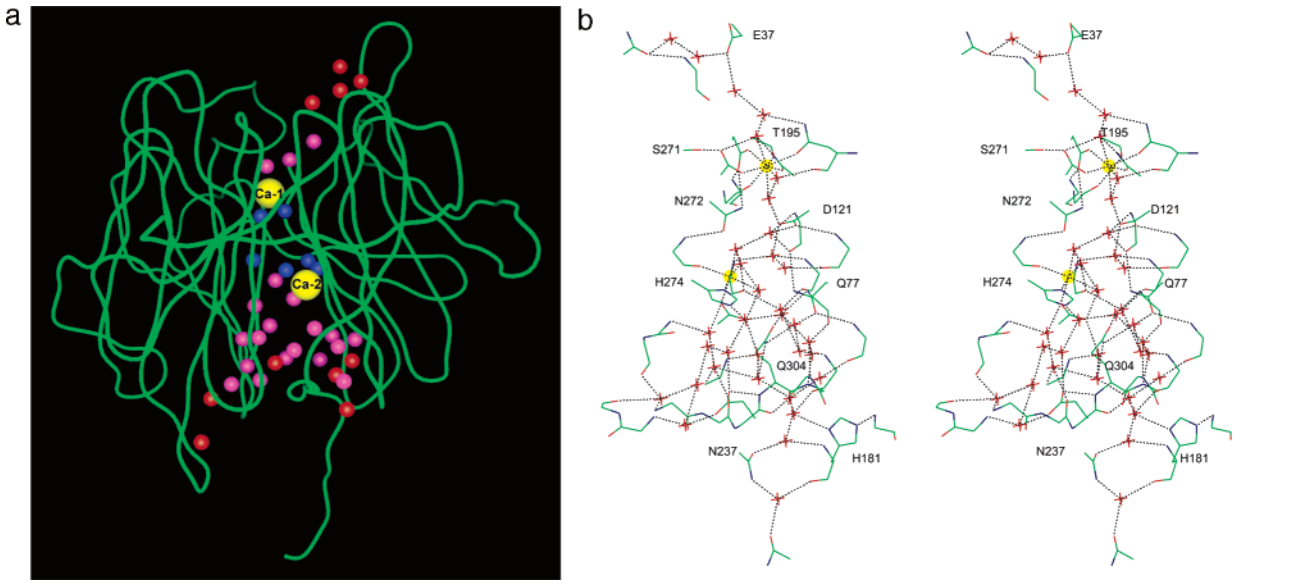

FIGURE 5: (a) Representation of the DFPase backbone fold, with the two calcium atoms and water molecules inside the central tunnel shown as spheres. Water molecules are color-coded according to the *B*-factor value: 5−6 Å^2 (blue), 6−10 Å^2 (magenta), or 10−15 Å^2 (red). [This picture was created with the program GRASP (*16*).] (b) Stereoview along the central tunnel of DFPase in the same direction as in panel a. The positions of the water molecules inside the tunnel are marked by red crosses; the two calcium atoms are represented by yellow spheres. The calcium coordinations and hydrogen bonds observed in the X-ray structure of the DFPase (PDB ID code 1PJX) are indicated by black dotted lines. Only for the hydrogen bond between WAT535 and WAT552, the bonded hydrogen atom is not observed in the ultra-high-resolution X-ray structure. [This picture was created with the program INSIGHT. All hydrogen bonds and calcium coordinations displayed in this figure are listed in detail in the Supporting Information (Table S3).]

Supporting Information) indicated that the protein fold remained intact in these mutants. In addition, [^{15}N,^{1}H]-TROSY experiments were performed with both mutant proteins; these two-dimensional heteronuclear NMR spectra showed that the fold of the proteins resembled the tertiary structure of the WT DFPase (see Figure S2 in the Supporting Information). However, the ^{15}N-labeled mutant N272F was considerably less stable than the WT protein, since it aggregated about 2 weeks after its preparation, whereas the ^{15}N-labeled mutant D121F behaved similarly to WT DFPase.

Hence, the mutants D121F and N272F show that the introduction of a bulky hydrophobic phenyl ring at position 121 or 272 inside the tunnel has a direct effect on the enzymatic reaction at the protein surface. Since the fold of both mutants remained unaffected, while the catalytic activity and one calcium atom were lost, it must be assumed that Ca-1 is the missing calcium atom. This effect, however, can only result from the disruption of the hydrogen bond network inside the central tunnel of DFPase, thus altering the electrostatics of the entire system. It appears that the more hydrophobic character and the greater space requirement of a phenyl ring in these two positions cause the loss of certain essential solvent molecules, in particular WAT604 or WAT623, which both directly coordinate calcium, thus leading to a destabilization of the calcium binding. Similar effects have been reported for other proteins such as human carboanhydrase II (*31*), the metallophosphatases calcineurin (*32*) and human serum transferrin (*33*), the *Eco*RV restriction endonuclease (*34*), as well as the 3,4-dihydroxybutanone-4-phosphate synthase from *Magnaporthe grisea* (*35*).

Ca-2 Binding Site. The high-affinity calcium-binding site of DFPase (Ca-2) is, at least in part, responsible for the structural stability of the DFPase (*2*). It is localized inside the central tunnel of the protein, coordinated octahedrally by residues Asp232, Leu273, and His274 as well as by the water molecules WAT509, WAT615, and WAT623. The dissociation constant of Ca-2 is below 5.3 nM (*2*), indicating that the calcium atom is well shielded from the bulk solution because of its protected position (*1*). Moreover, the imidazole ring of His274 displays an unusual calcium coordination, as N$^{\delta 1}$ is a direct Ca-2 ligand.

To explore the role of the negatively charged Asp232 side chain in the Ca-2 binding site, the mutant D232S was generated (Table 1). The introduction of a serine residue presumably leads to a different charge environment around Ca-2. Nevertheless, although the side chain carboxyl group, which acts as ligand of Ca-2, has been removed, the mutant D232S contains two calcium atoms and shows no significant structural differences to the typical fold of WT DFPase, based on a comparison of one-dimensional ^{1}H NMR spectra (see Figure S1 in the Supporting Information). Moreover, also the enzymatic activities of the mutant and WT protein are basically the same. To characterize the local structural changes caused by this replacement, the mutant D232S has been crystallized, and its X-ray structure was solved to a resolution of 1.1 Å. The mutant D232S displays several minor conformational changes in the Ca-2 binding site compared to the WT structure (Figure 6). The atom N$^{\delta 1}$ of His274 is shifted by 0.5 Å and the carbonyl oxygen of Leu273 by 1.14 Å. The isopropyl group of Leu273 is rotated by about 120° and the Ser232 C$^{\beta}$ atom is 0.74 Å displaced relative to Asp232 C$^{\beta}$. The side chain amide groups of Gln77 and Gln304 are each rotated by 90°. Moreover, Ser232 exhibits two distinct conformational states, whereby Ser232 O$^{\gamma}$ is rotated by about 120°. The existence of two different conformations of the Ser232 side chain suggests that a discrete disorder prevails in the Ca-2 binding site of the mutant D232S, which structurally also affects the Ca-2 coordination. In fact, the Ca-2 atom could not be assigned in the X-ray structure of this mutant; no corresponding

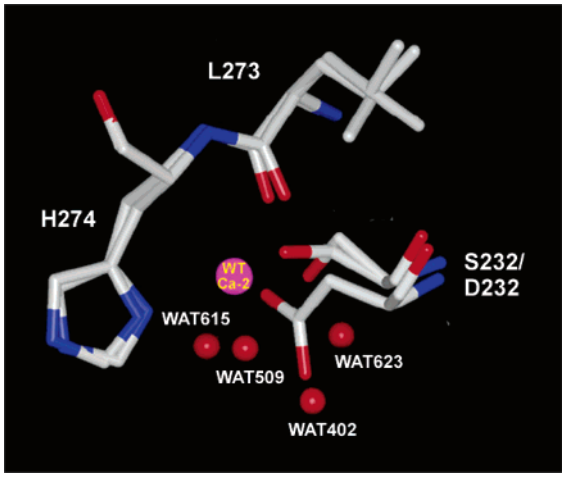

FIGURE 6: Superposition of the WT DFPase and the D232S X-ray structures. The protein ligands of Ca-2 are displayed as rods. In the mutant protein, two different conformations are observed for the S232 side chain, apparently due to discrete disorder. Likewise, Ca-2 (marked WT Ca-2) could be observed only in the WT structure, while WAT402 was found only in the mutant structure. [This picture was created with the program GRASP (*16*).]

electron density difference was detected at or near the position where Ca-2 is found in the WT structure. Instead, a water molecule (WAT402), which is not observed in the WT structure, was found in the mutant next to WAT509 and WAT623. Yet, the TXRF measurements showed that the mutant D232S does contain two calcium atoms. These results suggest that Ca-2 does exist, but is either bound with lower affinity or in a disordered state. In fact, the existence of two distinct Ser232 side chain conformations supports a less-defined coordination of Ca-2.

Remarkably, the double mutant D232S/S271A, consisting of both the D232S mutation (with 103% specific activity compared to WT DFPase) and the more active S271A mutation (134% compared to WT DFPase), showed no additive effect. Rather, this double mutant exhibited a 19% decrease in the specific activity compared to WT DFPase, indicating that the electrostatic effects governing the enzymatic activity of this system are rather complex.

His274, another Ca-2 ligand, exists in the energetically more favorable $N^{\epsilon 2}H$ protonation state, while $N^{\delta 1}$ coordinates the metal site. As expected, this histidine residue did not show any pH-titration behavior throughout the scanned pH range 5.76−9.45 (Table 2), since $N^{\delta 1}$ cannot be protonated. Moreover, the $N^{\epsilon 2}H$ resonance was detectable by NMR up to pH 9.04, demonstrating a slowed proton exchange that is apparently due to the very low solvent accessibility of His274, which is completely surrounded by fixated crystal waters that form the extensive hydrogen bond network inside the tunnel.

The H274N mutation (*3*) caused a 7% decrease in the specific activity (Table 1), again suggesting that changes inside the DFPase tunnel have an effect on the active site, which can only be relayed through the hydrogen bond network leading to the Ca-1 binding site.

Tunnel Residues Located beyond Ca-2. Next, we focused on residues found inside the central tunnel but located beyond Ca-2 relative to Ca-1. Gln77 and Gln304 are both positioned close to the Ca-2 binding site, whereas His181 and Asn237 are found at the far end of the tunnel.

The side chains of Gln77 and Gln304 both form a hydrogen bond to the same crystal water (WAT580) inside the tunnel. Hence, to disrupt the water-mediated hydrogen bond network in DFPase, Gln77 and Gln304 were each replaced by more bulky and highly hydrophobic residues. As shown in Table 1, the mutant Q77F was completely inactive and contained more than four calcium atoms per protein molecule, according to TXRF measurements. One-dimensional ^1H NMR spectra (see Figure S1 in the Supporting Information) furthermore indicated that this mutant protein was completely unfolded, thus explaining the high calcium content of this mutant. The insertion of such a large and completely hydrophobic side chain at this position apparently prevented the protein from adopting the correct three-dimensional fold. In contrast, the corresponding tryptophan and tyrosine mutants Q77W and Q77Y, which are both capable of forming hydrogen bonds, maintained the typical DFPase tertiary structure, as deduced from 1D ^1H NMR spectra (see Figure S1 in the Supporting Information) and the WT-like catalytic activity (Table 1).

Similarly, Gln304 was mutated to phenylalanine and tryptophan (Table 1). In this case, the mutant Q304W maintained full catalytic activity, possibly because of its ability to support hydrogen bonding, whereas the mutant Q304F lost about 50% of the WT catalytic activity, probably due to the disruption of the hydrogen bond network within the tunnel.

The mutation N237S has caused no significant changes in the enzymatic activity (Table 1). In contrast, the H181N mutation of the nearby His181 showed a remarkable reduction of the catalytic activity by 23% (Table 1), although the imidazole ring of this residue is located more than 18 Å away from Ca-1. This can only be explained by an electrostatic connection of residue 181 with the active site at the opposite end of the central DFPase tunnel. The substitution of H181 by N181 apparently affects the hydrogen bond network in the central tunnel of the DFPase. This would once again support the electrostatic influence of this tunnel-spanning water network on DFP catalysis.

Therefore, we focused more on the conformational properties of this residue. On the basis of the X-ray structure of WT DFPase, His181 is only about 3% accessible by the bulk solvent. Hydrogen bonds between His181 $N^{\epsilon 2}$ and Tyr126 NH as well as between His181 $N^{\delta 1}H$ and WAT703 have been deduced on the basis of distances and geometry in the X-ray structure. NMR data (Table 2) have confirmed that the imidazole ring of His181 exists in the energy-rich $N^{\delta 1}H$ tautomeric state; except for His248, which also occurs as a $N^{\delta 1}H$ conformer, all other histidine residues (His219, His224, His274, and His287) take on the energetically more favorable $N^{\epsilon 2}H$ form. Moreover, the imidazole ring of His181 did not titrate within the scanned pH range 5.76−9.45; aside from His287 in the active site and the Ca-2 ligand His274, which also showed no titration effects, all other histidine residues (His219, His224, and His248) were located at the protein surface and displayed pH-dependent changes in their imidazole ring resonances below pH 7. Additional evidence for a well-shielded position of His181 provides the fact that $N^{\delta 1}H$ showed slowed proton exchange for most of the scanned pH range (6.45−9.04), whereas the surface residues His219 and His224 exhibited fast proton exchange at all titration points (merely the $N^{\delta 1}H$ conformer of the solvent-exposed His248

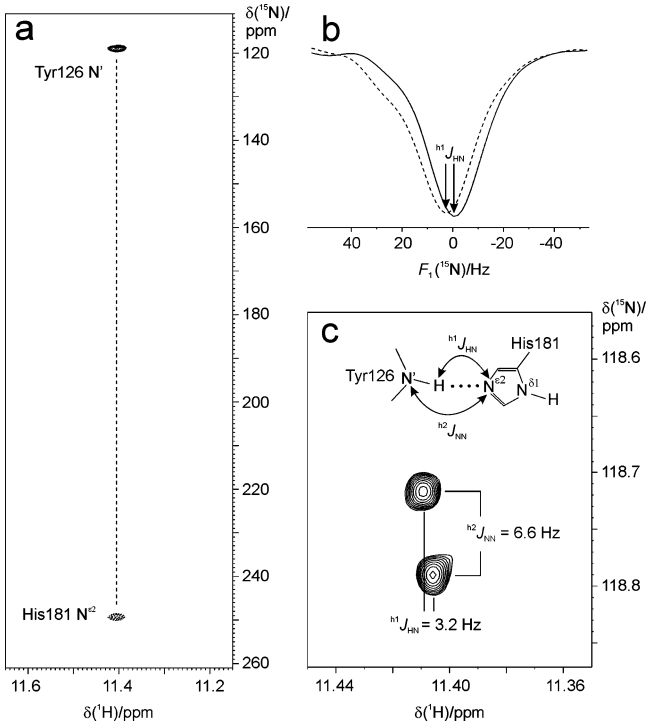

FIGURE 7: Measurement of trans-hydrogen-bond scalar couplings between the backbone amide group of Tyr126 and $N^{\epsilon 2}$ of His181 in WT DFPase. (a) Region from a 2D [^{15}N,^{1}H]-TROSY-H(N)N-COSY spectrum recorded with a *J*-transfer period of 40 ms. Positive and negative intensities are represented by solid and dashed contours, respectively. (b) Traces along the F_1 (^{15}N) dimension through the Tyr126−His181 cross-peak in a $^{1}H-S^{3}$ [^{15}N,^{1}H]-TROSY-H(N)N-COSY experiment. The solid (dashed) line is taken from the subspectrum recorded without (with) inversion of ^{1}H spins before and after the t_1 evolution period. Their frequency separation represents the $^{h1}J_{Tyr126H'-His181N^{\epsilon 2}}$ coupling constant, as indicated. (c) Section from a 900 MHz [^{15}N,^{1}H]-TROSY spectrum showing the E.COSY-like cross-peak of Tyr126. Horizontal and vertical displacements of the two multiplet components correspond to the $^{h1}J_{HN}$ and $^{h2}J_{NN}$ coupling constants, respectively.

could be detected, at pH values ≥7.89). Apparently, the hydrogen bond to WAT703 remains intact throughout a wide pH range, suggesting that this crystal water molecule, which is part of the tunnel-spanning hydrogen bond network, does not exchange.

The other hydrogen bond connects the His181 imidazole ring with Tyr126 HN. Using heteronuclear NMR spectroscopy, direct evidence for N−H···N hydrogen bridges can be obtained from the existence of two-bond $^{15}N-^{15}N$ and one-bond $^{1}H-^{15}N$ scalar couplings across the hydrogen bond (*23*, *24*). The HNN-COSY experiment (*23*) allows a correlation between nuclei on both sides of the hydrogen bridge via $^{h2}J_{NN}$ couplings. Its application to perdeuterated and ^{15}N-labeled DFPase is depicted in Figure 7a. As expected, the backbone amide of Tyr126 clearly showed a correlation to a ^{15}N resonance in the histidine side chain region. While backbone resonance assignments of DFPase were obtained using standard triple resonance methods, as reported previously (*36*), the assignment of the hydrogen bond acceptor nitrogen was achieved by a combination of NOESY and [^{15}N,^{1}H]-HMBC experiments (data not shown). From the intensity ratio between the Tyr126 H^N−His181 $N^{\epsilon 2}$ cross-peak and the Tyr126 autocorrelation peak, the magnitude of the $^{h2}J_{NN}$ interaction was calculated to be 5.7 Hz.

An electron-mediated coupling between the bridging hydrogen nucleus and the acceptor nitrogen can be observed using a related method (*24*), where magnetization is transferred to the acceptor nitrogen via $^{h2}J_{NN}$ coupling in order to measure ^{15}N frequency differences in subspectra representing the donor ^{1}H α and β spin states. Here, a version of the ^{1}H spin state-selective (S^3) HNN-COSY was employed, which selects for the TROSY component during both *J*-transfer periods and either leaves ^{1}H spin states unperturbed or inverts them immediately before and after the ^{15}N evolution time (*25*, *26*). A superposition of the corresponding cross sections through the Tyr126−His181 cross-peak is shown in Figure 7b. Their horizontal displacement yields a coupling constant $^{h1}J_{HN}$ of 3.3 Hz with a sign opposite, i.e., positive, to that of the regular $^{1}J_{HN}$ coupling of the Tyr126 autocorrelation peak (not shown), which is consistent with results obtained for nucleic acid base pairs (*24*−*26*, *37*).

Accurate values for both $^{h1}J_{HN}$ and $^{h2}J_{NN}$ can be obtained from a [^{15}N,^{1}H]-TROSY experiment recorded with high resolution in the ^{15}N dimension when excitation of the acceptor nitrogen is avoided (*28*), giving rise to an E.COSY-type (*38*) cross-peak pattern (Figure 7c). The $^{h1}J_{HN}$ coupling constant thus measured (3.2 Hz) is in good agreement with the result of the $^{1}H-S^{3}$ HNN-COSY experiment. In contrast, the associated $^{h2}J_{NN}$ splitting (6.6 Hz) is somewhat larger than the value derived from signal intensities in the HNN-COSY. Most likely, in the latter experiment the magnitude of the coupling is slightly underestimated due to the finite excitation bandwidth of the ^{15}N radio-frequency pulses.

CONCLUSIONS

The aim of this work was to (i) reexamine the proposed catalytic mechanism of DFPase (*1*) and (ii) identify residues that may be additionally involved in the catalytic reaction and/or substrate binding. The large number of single and double mutants generated during the course of this study provide several conclusions.

First, large hydrophobic residues in the major groove (in particular at positions 173, 195, and 244) are more favorable for substrate turnover than residues with small side chains. Second, a series of His287 mutations demonstrated that the catalytic reaction can take place without several requirements that had been postulated previously (*1*): (i) a hydrophobic residue (either aromatic or aliphatic) at position 287 is favorable for substrate turnover, while polar residues result in a significant loss of enzymatic activity, possibly because they bind the hydrolytic water molecule; (ii) the existence of a hydrogen bond between His287 and Trp244 is not essential but may be beneficial for the same reason, rendering the 287−244 system less polar; (iii) although an activation of the hydrolytic water molecule via proton abstraction by residue 287 is not crucial for the catalytic reaction (as demonstrated by the relatively high activities of mutants H287F, H287L, H287W, and H287Y), an imidazole ring may provide the highest specific activity because of its proton abstraction capability. Third, mutations of the Ca-1 ligands have revealed that the net charge at the Ca-1 binding site as well as the positional arrangement of the charged groups are important factors for the maintenance of the catalytic activity of the enzyme. Finally, the characterization of various residues inside the central DFPase tunnel by site-directed

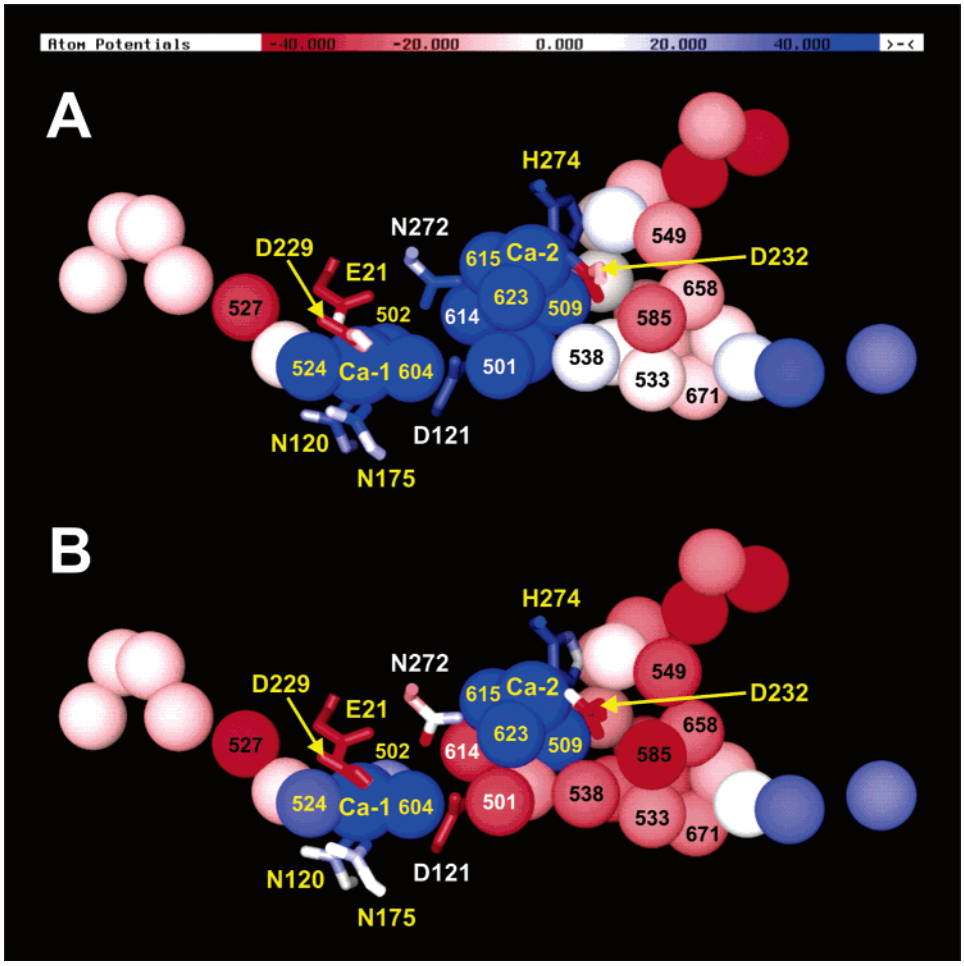

FIGURE 8: Atom potentials of the water molecules (spheres) as well as certain protein side chains (rods) that are part of the WT DFPase hydrogen bond network as displayed in Figure 5b. Waters are labeled according to WAT number either in yellow (direct calcium ligands), in white (located between Ca-1 and Ca-2), or in black. Amino acid side chains are labeled according to the same color code. Major differences in the atom potentials (in units of kT) are observed in dependence of the Asp121 protonation state: (A) uncharged Asp121 or (B) negatively charged Asp121. WAT501 and WAT614 (both hydrogen bond partners of Asp121) as well as neighboring waters spanning all the way to WAT549 are strongly affected. In the other direction, WAT604 (another hydrogen bond partner of Asp121 and direct Ca-1 ligand) appears to be unaffected, while the two water ligands of Ca-1 (WAT502 and WAT524) both show an effect that can be traced up to WAT527. [This picture was created with the program GRASP (*16*).]

mutagenesis showed that alterations in the hydrogen bond network can exert significant effects on the active site. In fact, the reduced specific activities of the mutants E37Q (56%) and H181N (81%), which are located at opposite ends of the central tunnel, emphasize that changes in the electrostatics of the system are relayed through the water-filled tunnel.

It is certainly difficult to envision how the electrostatic potentials of the tunnel residues may influence the substrate turnover at the active site. Figure 8 demonstrates the far-reaching effects that can occur due to a single charge alteration inside the DFPase tunnel. In WT DFPase, the double positive charge at Ca-1 is compensated by two negative charges (Glu21 and Asp229), whereas one full positive charge remains at Ca-2 where Asp232 is the only negatively charged ligand. Consequently, if the Asp121 carboxylate group (located between Ca-1 and Ca-2) is assumed to be uncharged (Figure 8, upper panel), the atom potentials of the water molecules and protein side chains between the two calcium-binding sites are predominantly positive, including Asp121. A negatively charged Asp121 side chain (Figure 8, lower panel), on the other hand, brings about drastic changes in the atom potentials well beyond both Ca-1 and Ca-2. The ultra-high-resolution X-ray data of WT DFPase presently suggest that the Asp121 carboxylate group is in fact deprotonated, i.e., negatively charged. Hence, even if the D121F mutation would not sterically disrupt the hydrogen bond network between Ca-1 and Ca-2, the charge difference between aspartate and phenylalanine should have a similarly drastic effect on the electrostatics in this tunnel system and, more importantly, on the electrostatic potentials in the active site.

We have presented cases here where mutations of residues lining the DFPase tunnel have diminished either the stability or the activity of the protein. Such implications are not unusual but had previously not been associated with DFPase, at least as far as the reaction mechanism is concerned. The stabilizing effects of water-mediated hydrogen bond networks in biomolecular systems are well-known. A hydrogen bond network that stabilizes the entire protein structure as well as the active site and metal binding sites has been described for several other proteins (*39*−*41*). In the case of alanine racemase, water molecules are involved in hydrogen bonding to other water molecules, thus creating an extensive hydrogen bond network that links the two monomers of the enzyme (*42*). Similar cases have been observed at the interfaces of

many other biological systems, where water molecules help in stabilizing the dimer interface (*43*, *44*). Aside from such structural effects, hydrogen bond networks in proteins have often also been described to play a crucial role in enzymatic catalysis, as in the case of HIV-1 protease, human manganese superoxide dismutase, and human heme oxygenase-1 (*45*−*47*). In thymidylate synthase, the disruption of the water-mediated hydrogen bond network by the introduction of a site-directed mutation resulted in an impairment of the catalytic reaction (*48*), similar to DFPase. It was realized early on that for understanding protein reaction mechanisms it would be necessary to consider the entire enzyme−substrate−solvent system. Warshel and Levitt (*49*), for example, reported that electrostatic stabilization of the carbonium ion intermediate is an important factor in the reaction mechanism of lysozyme. Electrostatic fields at the active sites of several other enzymes such as carboxypeptidase A, carbonic anhydrase, and acetylcholinesterase have been implicated in their functional efficiency (*50*−*52*). In the case of the Cu/Zn superoxide dismutase, the analysis of the three-dimensional electrostatic vector field showed that the arrangement of electrostatic charges promotes the enzyme−substrate interaction through substrate guidance; i.e., the electrostatic field directs the substrate toward the catalytic binding site (*53*). Hence, an interruption of a hydrogen bond network that is connected to the active site of an enzyme, as is the case in DFPase, can either cause a structural destabilization or, by altering the existing electrostatic potentials, affect the enzymatic reactivity.

ACKNOWLEDGMENT

We thank Juliana Winkler (University of Frankfurt) and Ralf Diem (Max Planck Institute of Biophysics) for excellent technical assistance in biochemical and X-ray experiments, respectively.

SUPPORTING INFORMATION AVAILABLE

Primers used for site-directed mutagenesis (Table S1), kinetic parameters of several DFPase mutants (Table S2), hydrogen bonds and calcium coordinations spanning the central tunnel of DFPase (Table S3), 1D ^{1}H NMR spectra of DFPase mutant samples (Figure S1), and 2D [^{15}N,^{1}H]-TROSY NMR spectra of D121F and wild-type DFPase (Figure S2). This material is available free of charge via the Internet at http://pubs.acs.org.

REFERENCES

1. Scharff, E. I., Koepke, J., Fritzsch, G., Lücke, C., and Rüterjans, H. (2001) Crystal structure of diisopropylfluorophosphatase from *Loligo vulgaris*, *Structure 9*, 493−502.
2. Hartleib, J., Geschwindner, S., Scharff, E. I., and Rüterjans, H. (2001) Role of calcium ions in the structure and function of the di-isopropylfluorophosphatase from *Loligo vulgaris*, *Biochem. J. 353*, 579−589.
3. Hartleib, J., and Rüterjans, H. (2001) Insights into the reaction mechanism of the diisopropyl fluorophosphatase from *Loligo vulgaris* by means of kinetic studies, chemical modification and site-directed mutagenesis, *Biochim. Biophys. Acta 1546*, 312−324.
4. Hartleib, J., and Rüterjans, H. (2001) High-yield expression, purification, and characterization of the recombinant diisopropylfluorophosphatase from *Loligo vulgaris*, *Protein Expression Purif. 21*, 210−219.
5. Landis, W. G., Haley, M. V., and Johnson, D. W. (1986) Kinetics of the DFPase activity in *Tetrahymena thermophila*, *J. Protozool. 33*, 216−218.
6. Landis, W., Haley, D., Haley, M. J. D., Dupont, H., and Savage, R. E., Jr. (1987) Discovery of multiple organofluorophosphate hydrolyzing activities in the protozoan *Tetrahymena thermophila*, *J. Appl. Toxicol. 7*, 35−41.
7. Josse, D., Xie, W., Renault, F., Rochu, D., Schopfer, L. M., Masson, P., and Lockridge, O. (1999) Identification of residues essential for human paraoxonase (PON1) arylesterase/organophosphatase activities, *Biochemistry 38*, 2816−2825.
8. La Du, B. N., Aviram, M., Billecke, S., Navab, M., Primo-Parmo, S., Sorenson, R. C., and Standiford, T. J. (1999) On the physiological role(s) of the paraoxonases, *Chem.-Biol. Interact. 119*−*120*, 379−388.
9. Cheng, T.-C., Liu, L., Wang, B., Wu, J., DeFrank, J. J., Anderson, D., Rastog, I. V. K., and Hamilton, A. B. (1997) Nucleotide sequence of a gene encoding an organophosphorus nerve agent degrading enzyme from *Alteromonas haloplanktis*, *J. Ind. Microbiol. 18*, 49−55.
10. Vanhooke, J. L., Benning, M. M., Raushel, F. M., and Holden, H. M. (1996) Three-dimensional structure of the zinc-containing phosphotriesterase with the bound substrate analog diethyl 4-methylbenzylphosphonate, *Biochemistry 35*, 6020−6025.
11. Scharff, E. I., Lücke, C., Fritzsch, G., Koepke, J., Hartleib, J., Dierl, S., and Rüterjans, H. (2001) Crystallization and preliminary X-ray crystallographic analysis of DFPase from *Loligo vulgaris*, *Acta Crystallogr. D57*, 148−149.
12. Koepke, J., Scharff, E. I., Lücke, C., Rüterjans, H., and Fritzsch, G. (2003) Statistical analysis of crystallographic data obtained from squid ganglion DFPase at 0.85 Å resolution, *Acta Crystallogr. D59*, 1744−1754.
13. Otwinowski, Z. (1993) Oscillation data reduction program, in *Data Collection and Processing* (Sawyer, L., Isaacs, N., and Bailey, S., Eds.) pp 56−62, Science and Engineering Research Council, Daresbury Laboratory, Warrington, U.K.
14. Minor, W. (1993) XDISPLAYF Program, Purdue University, West Lafayette, IN.
15. CCP4 (Collaborative Computational Project 4) (1994) The CCP4 suite: programs for protein crystallography, *Acta Crystallogr. D50*, 760−763.
16. Nicholls, A., Sharp, K. A., and Honig B. (1991) Protein folding and association: insights from the interfacial and thermodynamic properties of hydrocarbons, *Proteins 11*, 281−296.
17. Löhr, F., Katsemi, V., Betz, M., Hartleib J., and Rüterjans, H. (2002) Sequence-specific assignment of histidine and tryptophan ring ^{1}H, ^{13}C and ^{15}N resonances in ^{13}C/^{15}N- and ^{2}H/^{13}C/^{15}N-labelled proteins, *J. Biomol. NMR 22*, 153−164.
18. Pervushin, K., Riek, R., Wider, G., and Wüthrich, K. (1997) Attenuated T_2 relaxation by mutual cancellation of dipole−dipole coupling and chemical shift anisotropy indicates an avenue to NMR structures of very large biological macromolecules in solution, *Proc. Natl. Acad. Sci. U.S.A. 94*, 12366−12371.
19. Kay, L. E., Keifer, P., and Saarinen, T. (1992) Pure absorption gradient enhanced heteronuclear single quantum correlation spectroscopy with improved sensitivity, *J. Am. Chem. Soc. 114*, 10663−10665.
20. Czisch, M., and Boelens, R. (1998) Sensitivity enhancement in the TROSY experiment, *J. Magn. Reson. 134*, 158−160.
21. Pervushin, K., Wider, G., and Wüthrich, K. (1998) Single transition-to-single transition polarization transfer (ST2-PT) in [^{15}N,^{1}H]-TROSY, *J. Biomol. NMR 12*, 345−348.
22. Weigelt, J. (1998) Single scan, sensitivity- and gradient-enhanced TROSY for multidimensional NMR experiments, *J. Am. Chem. Soc. 120*, 10778−10779.
23. Dingley, A. J., and Grzesiek, S. (1998) Direct observation of hydrogen bonds in nucleic acid basepairs by internucleotide $^{2}J_{NN}$ couplings, *J. Am. Chem. Soc. 120*, 8293−8297.
24. Pervushin, K., Ono, A., Fernández, C., Szyperski, T., Kainosho, M., and Wüthrich, K. (1998) NMR scalar couplings across Watson−Crick base pair hydrogen bonds in DNA observed by transverse relaxation-optimized spectroscopy, *Proc. Natl. Acad. Sci. U.S.A. 95*, 14147−14151.
25. Yan, X., Kong, X., Xia, Y., Sze, K. H., and Zhu, G. (2000) Determination of internucleotide $^{h}J_{HN}$ couplings by the modified 2D J_{NN}-correlated [^{15}N, ^{1}H] TROSY, *J. Magn. Reson. 147*, 357−360.

26. Wu, Z., Ono, A., Kainosho, M., and Bax, A. (2001) H···N hydrogen bond lengths in double stranded DNA from internucleotide dipolar couplings, *J. Biomol. NMR 19*, 361−365.
27. Kupce, E., and Freeman, R. (1995) Adiabatic pulses for wideband inversion and broadband decoupling, *J. Magn. Reson., Ser. A 115*, 273−276.
28. Barfield, M., Dingley, A. J., Feigon, J., and Grzesiek, S. (2001) A DFT study of the interresidue dependencies of scalar *J*-coupling and magnetic shielding in the hydrogen-bonding regions of a DNA triplex, *J. Am. Chem. Soc. 123*, 4014−4022.
29. Watkins, L. M., Mahoney, H. J., McCulloch, J. K., and Raushel, F. M. (1997) Augmented hydrolysis of diisopropyl fluorophosphate in engineered mutants of phosphotriesterase, *J. Biol. Chem. 272*, 25596−25601.
30. Kuo, J. M., Chae, M. Y., and Raushel, F. M. (1997) Perturbations to the active site of phosphotriesterase, *Biochemistry 36*, 1982−1988.
31. DiTusa, C. A., McCall, K. A., Christensen, T., Mahapatro, M., Fierke, C. A., and Toone, E. (2001) Thermodynamics of metal ion binding. 2. Metal ion binding by carbonic anhydrase variants, *Biochemistry 40*, 5345−5351.
32. Mertz, P., Yu, L., Sikkink, R., and Rusnak, F. (1997) Kinetic and spectroscopic analyses of mutants of a conserved histidine in the metallophosphatases calcineurin and λ protein phosphatase, *J. Biol. Chem. 272*, 21296−21302.
33. He, Q. Y., Mason, A. B., Woodworth, R. C., Tam, B. M., MacGillivray, R. T. A., Grady, J. K., and Chasteen, N. D. (1998) Mutations at nonliganding residues Tyr-85 and Glu-83 in the N-lobe of human serum transferrin, *J. Biol. Chem. 273*, 17018−17024.
34. Vipond, I. B., Moon, B. J., and Halford, S. E. (1996) An isoleucine to leucine mutation that switches the cofactor requirement of the *Eco*RV restriction endonuclease from magnesium to manganese, *Biochemistry 35*, 1712−1721.
35. Liao, D. I., Zheng, Y. J., Viitanen, P. V., and Jordan, D. B. (2002) Structural definition of the active site and catalytic mechanism of 3,4-dihydroxy-2-butanone-4-phosphate synthase, *Biochemistry 41*, 1795−1806.
36. Löhr, F., Katsemi, V., Hartleib, J., Günther, U., and Rüterjans, H. (2003) A strategy to obtain backbone resonance assignments of deuterated proteins in the presence of incomplete amide $^{2}H/^{1}H$ back-exchange, *J. Biomol. NMR 25*, 291−311.
37. Dingley, A. J., Masse, J. E., Peterson, R. D., Barfield, M., Feigon, J., and Grzesiek, S. (1999) Internucleotide scalar couplings across hydrogen bonds in Watson−Crick and Hoogsteen base pairs of a DNA triplex, *J. Am. Chem. Soc. 121*, 6019−6027.
38. Griesinger, C., Sørensen, O. W., and Ernst, R. R. (1985) Two-dimensional correlation of connected NMR transitions, *J. Am. Chem. Soc. 107*, 6394−6396.
39. Davis, J. P., Zhou, M.-M., and Van Etten, R. L. (1994) Spectroscopic and kinetic studies of the histidine residues of bovine low-molecular-weight phosphotyrosyl protein phosphatase, *Biochemistry 33*, 1278−1286.
40. Petersen, B. Ø., and Shuman, S. (1997) Histidine 265 is important for covalent catalysis by vaccinia topoisomerase and is conserved in all eukaryotic type I enzymes, *J. Biol. Chem. 272*, 3891−3896.
41. Yuan, C., Byeon, I. J., Li, Y., and Tsai, M. D. (1999) Structural analysis of phospholipase A_2 from functional perspective. 1. Functionally relevant solution structure and roles of the hydrogen-bonding network, *Biochemistry 38*, 2909−2918.
42. Mustata, G., and Briggs, J. M. (2004) Cluster analysis of water molecules in alanine racemase and their putative structural role, *Protein Eng. 17*, 223−234.
43. Janin, J., and Chothia, C. (1990) The structure of protein−protein recognition sites, *J. Biol. Chem. 265*, 16027−16030.
44. Miller, M. D., and Krause, K. L. (1996) Identification of the *Serratia* endonuclease dimer: structural basis and implications for catalysis, *Protein Sci. 5*, 24−33.
45. Sirois, S., Prounov, E. I., Truchon, J. F., Tsoukas, C. M., and Salahub, D. R. (2003) A density functional study of the hydrogen-bond network within the HIV-1 protease catalytic site cleft, *J. Comput. Chem. 24*, 1110−1119.
46. Ramilo, C. A., Leveque, V., Guan, Y., Lepock, J. R., Tainer, J. A., Nick, H. S., and Silverman, D. N. (1999) Interrupting the hydrogen bond network at the active site of human manganese superoxide dismutase, *J. Biol. Chem. 274*, 27711−27716.
47. Lightning, L. K., Huang, H., Moënne-Loccoz, P., Loehr, T. M., Schuller, D. J., Poulos, T. L., and Ortiz de Montellano, P. R. (2001) Disruption of an active site hydrogen bond converts human heme oxygenase-1 into a peroxidase, *J. Biol. Chem. 276*, 10612−10619.
48. Sage, C. R., Rutenber, E. E., Stout, T. J., and Stroud, R. M. (1996) An essential role for water in an enzyme reaction mechanism: The crystal structure of the thymidylate synthase mutant E58Q, *Biochemistry 35*, 16270−16281.
49. Warshel, A., and Levitt, M. (1976) Theoretical studies of enzymic reactions: dielectric, electrostatic and steric stabilization of the carbonium ion in the reaction of lysozyme, *J. Mol. Biol. 103*, 227−249.
50. Hayes, D. M., and Kollman, P. A. (1976) Electrostatic potentials of proteins. 2. Role of electrostatics in a possible catalytic mechanism for carboxypeptidase A, *J. Am. Chem. Soc. 98*, 7811−7814.
51. Sheridan, R. P., and Allen, L. C. (1981) The active site electrostatic potential of human carbonic anhydrase, *J. Am. Chem. Soc. 103*, 1544−1550.
52. Gilson, M. K., Straatsma, T. P., McCammon, J. A., Ripoll, D. R., Faerman, C. H., Axelsen, P. H., Silman, I., and Sussman, J. L. (1994) Open "back door" in a molecular dynamics simulation of acetylcholinesterase, *Science 263*, 1276−1278.
53. Getzoff, E. D., Tainer, J. A., Weiner, P. K., Kollman, P. A., Richardson, J. S., and Richardson, D. C. (1983) Electrostatic recognition between superoxide and copper, zinc superoxide dismutase, *Nature 306*, 287−290.

BI0500675